

Analytical solution for maximal frictional two-layer exchange flow

By LI GU AND GREGORY A. LAWRENCE†

Department of Civil Engineering, University of British Columbia, Vancouver, BC, Canada V6T 1Z4

(Received 3 April 2003 and in revised form 9 May 2005)

The maximal steady frictional exchange flow through a rectangular channel of constant width is analysed within the context of internal hydraulics. A one-dimensional analytical solution to the fully nonlinear problem of two-layer frictional exchange is developed and shown to compare well with experimental and field data. The analytical solution gives the maximal exchange flow rate and the variation in the height of the density interface along the channel for the case of zero barotropic forcing. In contrast to the assumed constant interface slope of previous theoretical formulations of frictional exchange flows, the resulting density interface is found to be nonlinear and asymmetric. Both interfacial and bottom friction play important roles in determining the exchange flow rate. It is shown that the frictional effects are important even in relatively short channels.

1. Introduction

Exchange flows are often driven by a slight density difference due to temperature, salinity and/or sediment concentration variations across a constriction connecting two water bodies. The exchange flow through the Strait of Gibraltar, where less saline North Atlantic water flows into the Mediterranean at the surface and more saline Mediterranean water flows out at depth, has attracted considerable attention (Armi & Farmer 1985). Other examples include the exchange flows through: the Bosphorus and Dardanelles (Defant 1961; Gregg, Özsoy & Latif 1999); the Bab el Mandab (Smeed 2004); the Great Belt connecting the Baltic and North Seas (Ottesen-Hansen & Moeller 1990); and the Burlington Ship Canal connecting Hamilton Harbour with Lake Ontario (Lawrence *et al.* 2004).

Many features of exchange flows have been successfully modelled by the hydraulic theory of two-layer inviscid flows (Armi & Farmer 1986; Farmer & Armi 1986), in which the nonlinear inertial effects are considered. Studies of frictional exchange flows have often ignored the inertial effects (e.g. Anati, Assaf & Thompson 1977). However, under many circumstances, both frictional and inertial effects are important and both should be included in the theoretical formulation of exchange-flow problems. To include both effects, investigators have resorted to numerical techniques (Assaf & Hecht 1974; Oğuz *et al.* 1990; Zaremba, Lawrence & Pieters 2003).

This paper presents an analytical solution to the fully nonlinear problem of frictional two-layer exchange flow. After presenting the theoretical background in §2, the analytical solution is developed in §3. Laboratory experiments are presented in §4. The analytical solution is tested against the laboratory experiments and field data

† Author to whom correspondence should be addressed: lawrence@civil.ubc.ca.

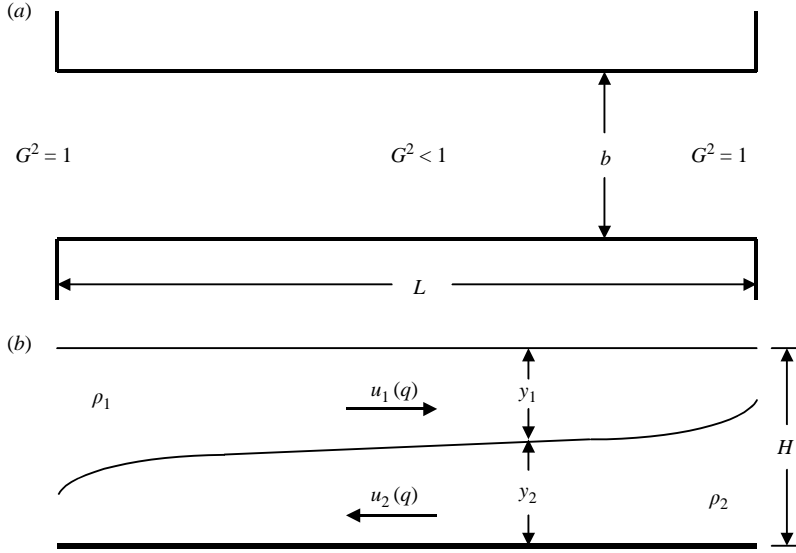


FIGURE 1. (a) Plan and (b) side views of the flow configuration for maximal two-layer exchange flow through a rectangular channel connecting two reservoirs of slightly different densities. H and b are total fluid depth and channel width, respectively. ρ_i , y_i and u_i are density, layer thickness and horizontal velocity for layer i , respectively. Subscript $i = 1$ represents the upper layer, while $i = 2$ represents the lower layer.

from the Burlington Ship Canal in §5. In §6, the effects of friction on the exchange rate and the longitudinal profile of the interface are discussed.

2. Theoretical background

Consider frictional two-layer exchange between two large reservoirs containing water of slightly different densities connected by a rectangular channel with a flat bottom, as depicted in figure 1. The flow is steady without barotropic forcing, and relative density difference between the two fluids is assumed to be small. This configuration is simple enough to allow an analytical solution while still resembling many natural exchange flows. Removing the complications of variable topography isolates the effects of friction.

Following Schijf & Schönfeld (1953) and Zaremba *et al.* (2003), the effects of friction in two-layer flows can be accounted for using:

$$\frac{dE_I}{dx} = S_f, \quad (1a)$$

where the internal energy,

$$E_I = y_2 + (u_2^2 - u_1^2)/2g', \quad (1b)$$

the friction slope,

$$S_f = \frac{1}{2}f_b F_2^2 + \frac{1}{2}f_l \frac{(\Delta u)^2 H}{g' y_1 y_2} + \frac{f_w}{b} (F_1^2 y_1 + F_2^2 y_2), \quad (1c)$$

and the layer Froude numbers,

$$F_i^2 = u_i^2 / g' y_i \quad (i = 1, 2), \quad (1d)$$

where x is the horizontal distance from the left-hand end of the channel of width b . The subscript $i = 1$ represents the upper layer, and $i = 2$ the lower layer. The layer densities, depths and average velocities are represented by ρ_i , y_i and u_i , respectively, and the velocity shear between the two layers $\Delta u = u_1 - u_2$. The reduced acceleration due to gravity, $g' = \varepsilon g$, where $\varepsilon = (\rho_2 - \rho_1)/\rho_2$. We focus on flows with $\varepsilon \ll 1$ and $F_i^2 = O(1)$, which allows us to make the rigid-lid approximation that the total depth $H = y_1 + y_2$ is constant (Lawrence 1993). The bottom, interfacial and sidewall frictional factors are given by:

$$f_b = \frac{-2\tau_b}{\rho_2 u_2 |u_2|}, \quad f_I = \frac{2\tau_I}{\bar{\rho} \Delta u |\Delta u|}, \quad f_w = \frac{-2\tau_w}{\rho_i u_i |u_i|}, \quad (2a-c)$$

where τ_b , τ_I and τ_w are bottom, interfacial and sidewall shear stress, respectively, and $\bar{\rho} = (\rho_1 + \rho_2)/2$ is the mean density.

For a channel of constant width, substituting the equation for internal energy (1b) into (1a) yields the differential equation for the slope of the interface:

$$\frac{dy_2}{dx} = \frac{S_f}{1 - G^2}, \quad (3)$$

where the composite Froude number $G^2 = F_1^2 + F_2^2$ (Armi 1986). Two-layer flow is said to be supercritical, critical, or subcritical depending on whether G^2 is greater than, equal to, or less than unity. In the present study, we will assume maximal exchange (Armi & Farmer 1986) where the flow is critical at either end of the channel, i.e.

$$G^2 = F_1^2 + F_2^2 = 1 \quad \text{at } x = 0, L, \quad (4)$$

where L is the channel length. Strictly speaking, all the Froude numbers in the above equations should be multiplied by the momentum correction factor (Henderson 1966), however, for the flows we are considering, the correction is small compared with other uncertainties and will be neglected.

3. Analytical solution

The objective of this section is to solve (3) and (4) simultaneously to obtain the variation in interface position along the length of the channel and the exchange flow rate. A wide channel is assumed so that sidewall friction can be neglected. We adopt the convention that flow is from left to right in the upper layer, so u_1 is always positive, and flow is from right to left in the lower layer, so u_2 is always negative. For steady flow without barotropic forcing, the two-dimensional exchange flow rate,

$$q = u_1 y_1 = -u_2 y_2. \quad (5a, b)$$

The problem is simplified by using the following non-dimensional parameters:

$$y_1^* = \frac{y_1}{H}, \quad y_2^* = \frac{y_2}{H}, \quad E_I^* = \frac{E_I}{H}, \quad \chi = \frac{x}{L}, \quad (6a-d)$$

where the asterisks in y_1^* , y_2^* and E_I^* will be dropped hereinafter. The non-dimensional interfacial deflection from mid-depth ($y_2 = y_1 = 1/2$), η , is defined as:

$$\eta = y_2 - \frac{1}{2} = \frac{1}{2} - y_1. \quad (7)$$

The non-dimensional flow rate is represented by the composite Froude number when $\eta = 0$:

$$G_0 = \frac{4q}{\sqrt{g'H^3}}. \quad (8)$$

Following Anati *et al.* (1977) and Zaremba *et al.* (2003), we parameterize the frictional effects using:

$$\alpha = \frac{f_b L}{H}, \quad r_l = \frac{f_l}{f_b}. \quad (9a, b)$$

Note that the exchange flow problem, as we have defined it, is completely prescribed by α and r_l .

In terms of these non-dimensional parameters the interface slope equation, (3), becomes:

$$\frac{d\eta}{d\chi} = \frac{\alpha G_0^2 [(1 - 2\eta)^3 + 8r_l]}{4(1 - 4\eta^2)^3 - 4G_0^2(1 + 12\eta^2)}, \quad (10)$$

and the equation for critical flow at the exits, (4), becomes:

$$G^2 = \frac{G_0^2}{16(\frac{1}{2} - \eta_j)^3} + \frac{G_0^2}{16(\frac{1}{2} + \eta_j)^3} = 1 \quad (j = 0, 1), \quad (11)$$

where the subscript $j = 0$ represents the left-hand side channel exit ($\chi = 0$), and $j = 1$ the right-hand side channel exit ($\chi = 1$). Note that if η_0 is a solution to (11), then $\eta_1 = -\eta_0$.

For the sake of simplicity, we will assume that the friction ratio, $r_l = 1$, for the remainder of this section. The general results are presented in the Appendix, they have the same form as those presented here, but are considerably longer. Integrating (10) yields the following expression for the variation in interface elevation:

$$\alpha G_0^2 \chi = a_0 + 4\eta + 12\eta^2 + 16\eta^3 + 8\eta^4 + a_1 \ln(-\eta + \frac{3}{2}) + a_2 \left[\frac{1}{3} \ln(\eta^2 + \frac{3}{4}) - \frac{2}{\sqrt{3}} \tan^{-1} \left(\frac{-2\eta}{\sqrt{3}} \right) \right], \quad (12)$$

where a_0 is the constant of integration, $a_1 = \frac{2}{3}(7G_0^2 + 128)$, and $a_2 = \frac{1}{3}(2G_0^2 + 16)$. Before we can use (12) to obtain the variation in η along the channel, we must determine the flow rate (G_0) and the interface elevation at the control points at each end of the channel (η_0, η_1).

3.1. Determination of G_0, η_0 and η_1

The exchange flow problem is now expressed in terms of four equations ((11) and (12) at each end of the channel), in four unknowns, a_0, η_0, η_1 and G_0 . Taking the equation obtained by substituting $\eta = \eta_0$ at $\chi = 0$ into (12), and subtracting the equation obtained by substituting $\eta = \eta_1 = -\eta_0$ at $\chi = 1$ into (12), we eliminate the integration constant a_0 and obtain the relationship between G_0^2 and η at $\chi = 0$:

$$G_0^2 = \frac{-72\eta_0 - 32\eta_0^3 + \frac{256}{3} \ln \left[\frac{\eta_0 + \frac{3}{2}}{-\eta_0 + \frac{3}{2}} \right] - \frac{32}{\sqrt{3}} \tan^{-1} \left[\frac{4\sqrt{3}\eta_0}{-4\eta_0^2 + 3} \right]}{\alpha - \frac{14}{3} \ln \left[\frac{\eta_0 + \frac{3}{2}}{-\eta_0 + \frac{3}{2}} \right] + \frac{4}{\sqrt{3}} \tan^{-1} \left[\frac{4\sqrt{3}\eta_0}{-4\eta_0^2 + 3} \right]}. \quad (13)$$

The relationship between G_0^2 and η at $\chi = 1$ is obtained by substituting $\eta_0 = -\eta_1$ into (13):

$$G_0^2 = \frac{72\eta_1 + 32\eta_1^3 + \frac{256}{3} \ln \left[\frac{-\eta_1 + \frac{3}{2}}{\eta_1 + \frac{3}{2}} \right] - \frac{32}{\sqrt{3}} \tan^{-1} \left[\frac{-4\sqrt{3}\eta_1}{-4\eta_1^2 + 3} \right]}{\alpha - \frac{14}{3} \ln \left[\frac{-\eta_1 + \frac{3}{2}}{\eta_1 + \frac{3}{2}} \right] + \frac{4}{\sqrt{3}} \tan^{-1} \left[\frac{-4\sqrt{3}\eta_1}{-4\eta_1^2 + 3} \right]}. \quad (14)$$

The equation relating G_0^2 and η at each end of the channel is obtained by rearranging (11):

$$\eta_j^6 - \frac{3}{4}\eta_j^4 + \frac{3}{16}(G_0^2 + 1)\eta_j^2 + \frac{1}{64}(G_0^2 - 1) = 0. \quad (15)$$

Substituting $\eta_j^2 \equiv \omega + 1/4$ into (15) yields:

$$\omega^3 + \frac{3G_0^2}{16}\omega + \frac{G_0^2}{16} = 0. \quad (16)$$

Equation (16) has one real root and two imaginary roots. The real root is:

$$\omega = \frac{1}{2} \left[\sqrt{\left(\frac{G_0^2}{4}\right)^3 + \left(\frac{G_0^2}{4}\right)^2} - \frac{G_0^2}{4} \right]^{1/3} - \frac{1}{2} \left[\sqrt{\left(\frac{G_0^2}{4}\right)^3 + \left(\frac{G_0^2}{4}\right)^2} + \frac{G_0^2}{4} \right]^{1/3}. \quad (17)$$

Setting $\eta_1 = +\sqrt{\omega + 1/4}$ and $\eta_0 = -\sqrt{\omega + 1/4}$ gives:

$$\eta_0 = \pm \sqrt{\frac{1}{2} \left[\sqrt{\left(\frac{G_0^2}{4}\right)^3 + \left(\frac{G_0^2}{4}\right)^2} - \frac{G_0^2}{4} \right]^{1/3} - \frac{1}{2} \left[\sqrt{\left(\frac{G_0^2}{4}\right)^3 + \left(\frac{G_0^2}{4}\right)^2} + \frac{G_0^2}{4} \right]^{1/3} + \frac{1}{4}}. \quad (18)$$

Equations (13), (14) and (18) are illustrated graphically on the (G_0^2, η) -plane (figure 2). The critical flow curve, (18), is a symmetrical bell-shaped curve separating the supercritical ($G^2 > 1$) and subcritical ($G^2 < 1$) flow regimes. The area within the curve represents subcritical flow, while the area outside the curve represents the supercritical flow regime. If, for example, we take $\alpha = 0.1$ and $r_I = 1$, then points a and b represent intersections of (13) and (14) with $G^2 = 1$ at $\chi = 0$ and $\chi = 1$, respectively. The vertical coordinates of points a and b on the η -axis represent η_0 and η_1 , respectively, and the horizontal coordinates of both points gives G_0^2 representing the resulting maximal exchange flow rate. With increasing friction, the interface height at the right-hand exit increases and at the left-hand exit decreases, corresponding to the decreased exchange flow rate. Since the $G^2 = 1$ curve always intersects the crests of (13) and (14) on the (G_0^2, η) -plane, the exchange flows bounded by two controls at each end indeed represent the maximal exchange conditions. The resulting maximal exchange rates for $\alpha = 0.01, 0.1, 1.0$ and 10 ($r_I = 1$) are $G_0 = 0.915, 0.708, 0.371$ and 0.137 , respectively. Friction certainly reduces the exchange rate, but provided the fundamental requirement for maximal exchange is met, the maximal possible exchange rate is still achieved under given frictional conditions (Armi & Farmer 1987).

3.2. Variation in interface elevation along the channel

To solve for the interface position along the channel, the constant of integration a_0 is calculated by substituting G_0^2 and either η_0 at $\chi = 0$ or η_1 at $\chi = 1$ into (12). This yields a uniquely defined longitudinal interface profile. In figure 3(a), density interface

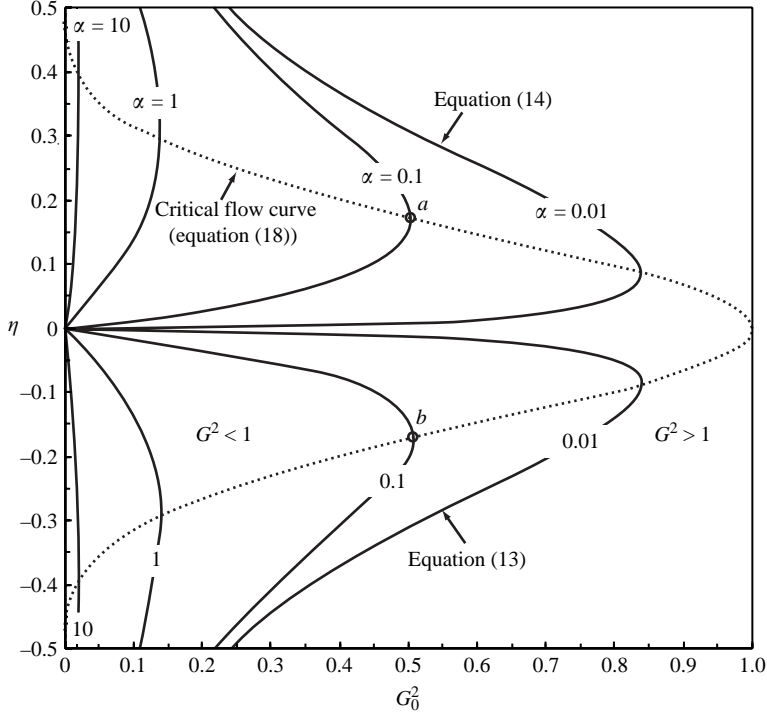


FIGURE 2. Presentation of maximal exchange flow solutions in the (G_0^2, η) -plane, where solid lines are solution curves of varying frictional parameters α ($r_l = 1$), the dotted line represents the critical boundary condition at each end of the channel. The intersections of solution curves with $G_0^2 = 1$ represent the values of G_0^2 and η at each end of the channel.

positions along the channel are shown for varying frictional effects ($\alpha = 0.01, 0.1, 1.0$ and 10). In the absence of surface friction, the interface is always slightly above the mid-depth at the centre of the channel. Given the exchange rates and interface positions, variations of other important flow parameters within the channel can also be obtained. Figure 3(b) shows the variations in the composite Froude number along the channel. The maximal exchange flow is critical at both ends of the channel ($G^2 = 1$). Within the channel, the composite Froude number drops below unity, representing subcritical flow conditions, the higher the friction the lower the composite Froude number at a given location.

3.3. Representation of solution on the Froude-number plane

The maximal frictional exchange flow solutions can also be represented on Armi's (1986) Froude-number (F_1^2, F_2^2) -plane. Following Armi (1986), the non-dimensional layer thickness can be expressed as follows:

$$y_1 = \left(\frac{G_0^2}{16F_1^2} \right)^{1/3}, \quad y_2 = \left(\frac{G_0^2}{16F_2^2} \right)^{1/3}. \quad (19)$$

Combining (19) with the rigid-lid approximation leads to the continuity equation in the Froude-number plane:

$$F_1^{-2/3} + F_2^{-2/3} = \left(\frac{G_0^2}{16} \right)^{-1/3}. \quad (20)$$

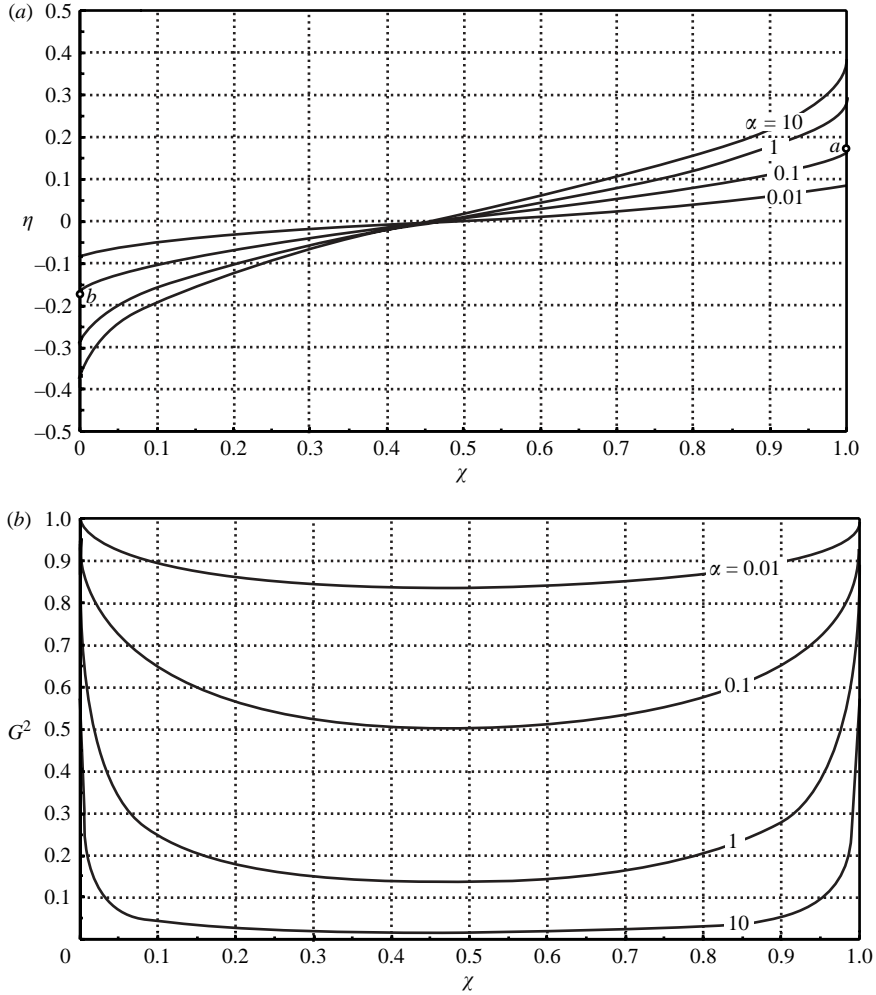


FIGURE 3. (a) Variation of density interface along the channel for maximal exchange with varying frictional parameters. Points a and b correspond to locations shown in figure 2. (b) Variation of the composite Froude number along the channel for maximal exchange with varying frictional parameters. The interfacial frictional factor is equal to the bottom frictional factor ($r_I = 1$) for both plots.

The internal energy is rewritten in terms of F_1^2 and F_2^2 :

$$E_I = \frac{F_2^{-2/3} \left(1 + \frac{1}{2} F_2^2\right) - \frac{1}{2} F_1^{-2/3} F_1^2}{F_1^{-2/3} + F_2^{-2/3}}. \quad (21)$$

In figure 4, contours of constant G_0 are superimposed on constant E_I contours on the (F_1^2, F_2^2) -plane depicting changes of internal energy and possible internal Froude number pairs as the interface varies along the channel. The critical condition ($G^2 = 1$) falls to a straight line separating supercritical and subcritical flows. For frictional exchange flows, the interface is tilted and the internal energy reduces monotonically from right to left along the channel. Each G_0 contour intersects with $G^2 = 1$ twice at different values of E_I when $G_0 < 1$. These two intersections, shown as hollow circles in

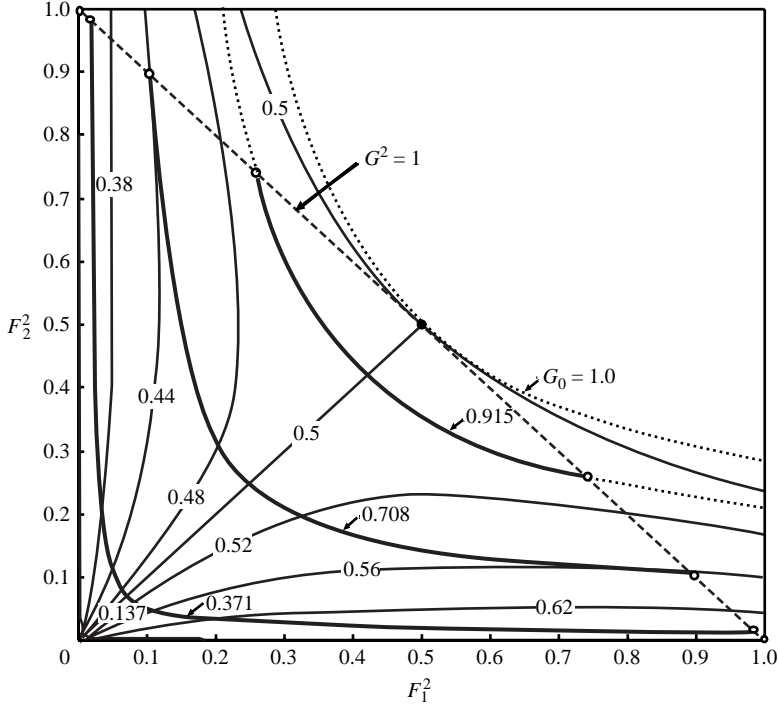


FIGURE 4. Maximal frictional exchange-flow solutions represented on the Froude-number (F_1^2, F_2^2)-plane, where contours of G_0 (thick lines) are superimposed on constant internal energy contours (thin lines). Contours of $G_0 = 0.915, 0.708, 0.371$ and 0.137 correspond to maximal frictional exchange solutions for $\alpha = 0.01, 0.1, 1$ and 10 , respectively ($r_l = 1$). The two symbols on each of the three G_0 contour lines represent flow conditions at the channel exits.

figure 4, represent two controls at either channel exit for maximal frictional exchange. Subcritical flow within the channel is represented by the G_0 curve between the controls.

When the flow is inviscid, the upper and lower layers are of equal thickness ($\eta = 0$) throughout the channel, and the flow is critical throughout the channel ($F_1^2 = F_2^2 = 0.5$). This flow condition, shown as the solid circle in figure 4, essentially depicts the solution of the lock-exchange problem of Wood (1970). The dimensional flow rate for inviscid flow is $\sqrt{g'H^3}/4$, so $G_0 = 4q/\sqrt{g'H^3}$ represents the ratio between the maximal frictional and inviscid exchange flow rates.

4. Laboratory experiments

Laboratory experiments were conducted in a 370 cm long and 106 cm wide tank divided into two reservoirs connected by a straight channel 200 cm long, 15.2 cm wide and 30 cm deep, with zero bottom slope (figure 5a). The front panel of the channel is made of Plexiglas, enabling observation of the flow. Salt was dissolved in the right-hand reservoir to make it slightly denser, so the upper layer flows from left to right, while the lower layer flows from right to left. Removing a barrier separating the two reservoirs started the experiments. After an initial start-up period, a maximal two-way exchange with internal hydraulic controls at both ends of the channel was established. The position of the interface throughout the channel was visualized by dissolving a fluorescent dye into the lower layer (figure 5b). Particle image velocimetry (Stevens & Coates 1994) was used to obtain the velocity profile. The exchange flow rate was

Experiment	g' (cm s ⁻²)	q (cm ² s ⁻¹)	G_0	K ($\chi = 0.5$)	f_b	α
1	0.27	14.3	0.74	1700	0.0132	0.094
2	0.49	20.2	0.78	3000	0.0127	0.091
3	0.72	24.0	0.76	3200	0.0116	0.083
4	0.95	28.5	0.79	4400	0.0108	0.077
5	1.14	30.9	0.78	4600	0.0104	0.074
6	1.33	32.4	0.76	4300	0.0095	0.068
7	1.61	36.4	0.78	5200	0.0083	0.059
8	1.83	39.4	0.79	5900	0.0071	0.051

TABLE 1. List of laboratory experiments.

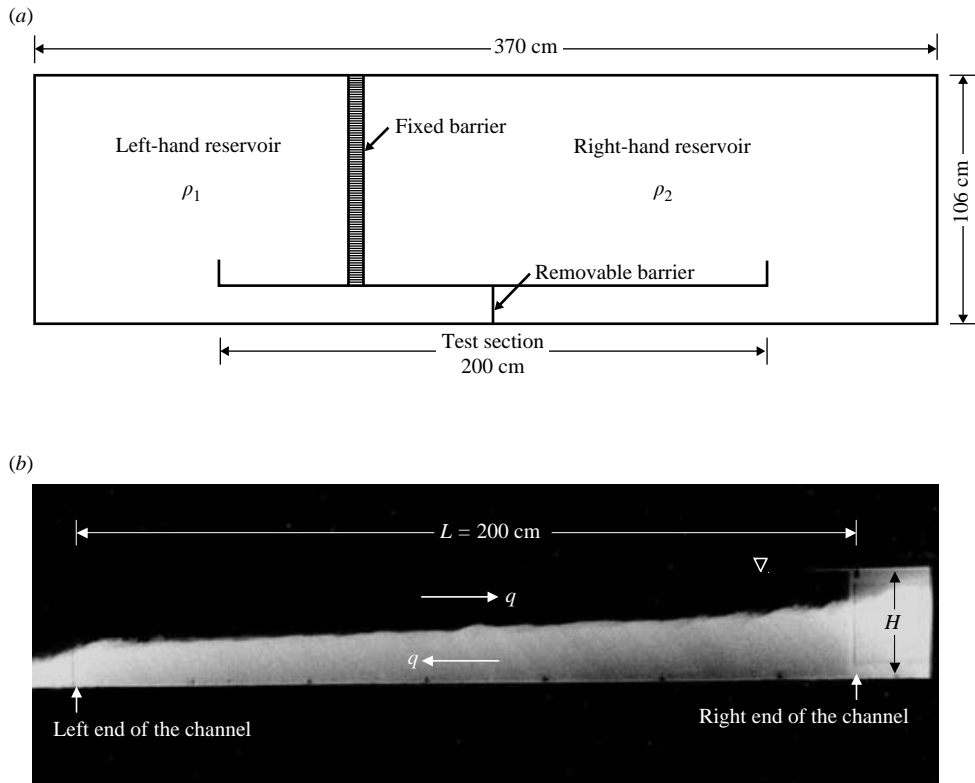


FIGURE 5. (a) Plan view of laboratory experiment set-up. (b) Laser-induced fluorescence image showing two-way maximal exchange flow.

obtained by integrating the velocity profile throughout the depth of the fluid. The average bottom and sidewall friction factors were estimated using the methodology of Zhu & Lawrence (2000).

A total of eight experiments were conducted (table 1). Throughout the experiments, the total fluid depth H was kept constant at 28.0 cm, while the reduced gravity g' was varied from 0.27 to 1.83 cm s⁻². The Keulegan number $K = \Delta u^3 / \nu g'$ calculated using the velocity shear Δu at $\chi = 0.5$ varies from 1700 to 5900. Since the velocity shear changes throughout the channel, this parameter varies slightly along the channel. The velocity shear increases towards the ends of the channel so K is always

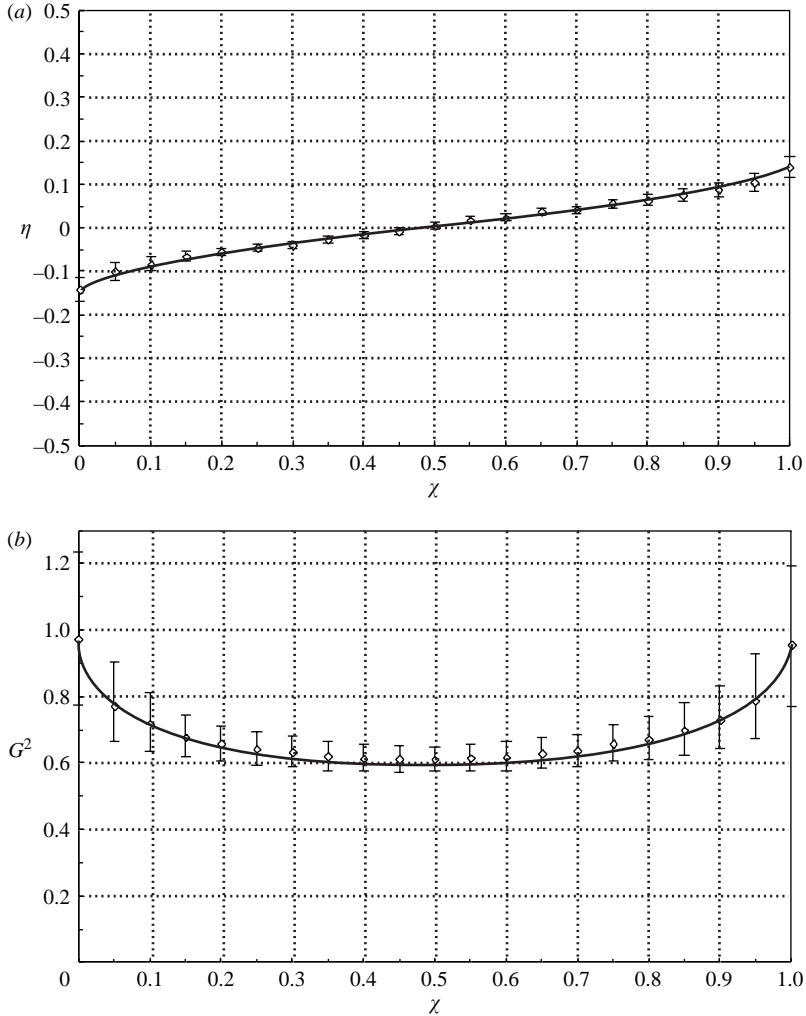


FIGURE 6. Comparison of results of experiment 5 with theoretical predictions ($\alpha = 0.074$ and $r_I = 0.79$). (a) Density interface position along the channel. (b) The variation of the composite Froude number along the channel. Symbols with error bars represent laboratory measurements and solid lines are theoretical predictions.

significantly higher than its critical value, which is in the range of 180 (Turner 1973) to 350 (Browand & Winant 1973), indicating an unstable density interface. The bulk Richardson number $J = (\Delta u)^2 / g'h \approx 0.3$ (where h is the shear-layer thickness), and the density interface is sharper than, and is generally displaced with respect to, the velocity interface, indicating the presence of one-sided Holmboe instabilities (Lawrence, Browand & Redekopp 1991). While Holmboe interfacial instabilities were present in the experiments, they are not as pronounced as those studied by Zhu & Lawrence (2001).

The major source of error in the experiments is in the determination of G_0 , the error is due in part to errors in determining the flow rate, but mostly due to the difficulty in determining the interface level, particularly at the ends of the channel where interfacial instabilities cause relatively large fluctuations in the interface level η (figure 6a). The fluctuations of G about the mean were approximately 10% at the ends of the channel and 2% in the centre of the channel, as shown in figure 6b.

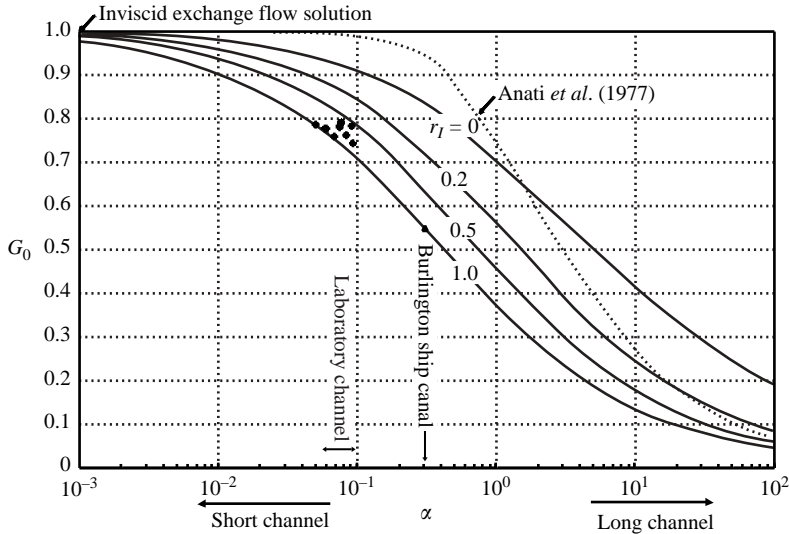


FIGURE 7. Frictional effects on exchange rate. The solid lines represent the analytical maximal exchange flow solutions through a wide channel. The symbols represent the laboratory experimental data and the field measurements in the Burlington Ship Canal.

5. Comparison of analytical solution with laboratory and field observations

This section aims to compare predictions of the analytical solution with the laboratory experiments and observations from the Burlington Ship Canal, a man-made canal connecting Lake Ontario with Hamilton Harbour. The analytical solution assumes a wide channel, where the sidewall friction is negligible. Although such an assumption is generally sound for natural channels, including the Burlington Ship Canal, it is not the case for the laboratory channel. To incorporate sidewall friction into the analysis, Gu (2001) introduced an equivalent interfacial friction factor:

$$f_{le} = f_l + \frac{H}{4b} f_w, \quad (22a)$$

and an equivalent friction ratio:

$$r_{le} = \frac{f_{le}}{f_b}. \quad (22b)$$

In the laboratory experiments, the depth to width ratio $H/4b = 0.46$, so sidewall friction is likely to be important.

The interfacial friction factor cannot be predicted with any accuracy from bulk flow properties, largely because the manner in which interfacial instabilities influence the value of f_l is still not well understood (Lawrence, Haigh & Zhu 1998). Estimates of f_l were obtained indirectly for each of the experiments. Estimates of f_b , obtained using the methodology of Zhu & Lawrence (2000), and G_0 were used in conjunction with the theoretical formulae (see Appendix) to obtain estimates of r_{le} . The comparison between the theoretical and laboratory results is presented in figure 7. Analysis of the eight experiments yielded an average value of $r_{le} = 0.79$ with a standard deviation of 0.18. Using the average value in conjunction with (22) yields $f_l = 0.33 f_b$, which from table 1 ranges from 0.0024 to 0.0044. These results are comparable with those obtained in laboratory experiments with similar parameter ranges (e.g. Sargent & Jirka 1987; Arita & Jirka 1987). The results quoted in Zhu & Lawrence (2000)

appear to be significantly higher, but the f_I quoted in that paper is equivalent to f_{Ie} in the present paper.

The measured interface elevations and composite Froude number are compared with predictions, using $\alpha = 0.074$ and $r_{Ie} = 0.79$ in figure 6. The agreement is excellent along the entire length of the channel. The mean values of the composite Froude number are slightly less than unity at both ends of the channel. This discrepancy is well within experimental error, but could, in fact, be real (see Garrett & Gerdes 2003). The composite Froude numbers are slightly higher than predicted in the centre of the channel, but again are within experimental error. Both the predicted and measured interfaces are very slightly above the mid-depth at the centre of the channel in the absence of surface friction. This effect is discussed in more detail in §6.2.

The Burlington Ship Canal is 836 m long and 89 m wide with an average depth of 10.7 m, connecting Hamilton Harbour with Lake Ontario. During the summer, contrast in density between the warm harbour water and the cool lake water drives an exchange flow, with a oscillating barotropic component due to surface seiches. Dick & Marsalek (1973) determined that $f_b \approx 0.0039$, which gives $\alpha \approx 0.3$. From Acoustic Doppler Current Profiler (ADCP) measurements in July 1996, Lawrence *et al.* (2004) calculate an average $G_0 = 0.55$ with a standard deviation of 0.08. Comparison of these values with the theoretical solution yields $r_I \approx 1.0$ (figure 7) and $f_I \approx 0.0039$. This result is encouraging since estimates of the Reynold's stress, obtained from analysis of ADCP data, give $f_I \approx 0.004$ (Lawrence *et al.* 2004).

The linear frictional exchange flow solution of Anati *et al.* (1977) is also included in figure 7 for comparison. Their model was developed for exchange flows through long channels, where frictional effects are dominant over nonlinear inertial effects. Furthermore, Anati *et al.* (1977) ignored interfacial friction and assumed the density interface followed a straight line linking the two hydraulic controls. This solution overestimates the exchange flow in shorter channels where inertial effects are more important. For long channels, the assumption of a constant interface slope prevents the solution of Anati *et al.* (1977) from converging to the nonlinear analytical solution even when interfacial friction is neglected ($r_I = 0$).

6. Discussion

6.1. Effects of friction on exchange rates

The frictional parameter α has been widely used as the indicator of the relative importance of frictional effects to inertial effects. If $\alpha \ll 1$, inertial effects dominate, and the channel is considered to be short. If $\alpha \gg 1$, friction dominates, and the channel is considered to be long. Finally, if $\alpha \approx 1$, both frictional and inertial forces are important, and the channel is considered to be marginal. However, the reduction in exchange rate can be significant even in short channels, as shown in figure 7. In each of the laboratory experiments $\alpha < 0.1$, yet the flow rate is reduced by more than 20 % in each case. For the Burlington Ship Canal with $\alpha = 0.3$ and $r_I = 1.0$, $G_0 = 0.55$. In this case, bed friction is responsible for a reduction of 17 % in exchange rate, whereas interfacial friction accounts for a reduction of 28 %. Thus, both α and r_I are important in determining the exchange rate.

To examine the relative importance of interfacial and bottom friction, it is useful to separate the interfacial friction and bottom friction slopes from the total friction slope S_f . For wide channels, the total friction slope can be expressed as the sum of the interfacial friction slope (S_{fI}) and the bottom friction slope (S_{fb}) in the following

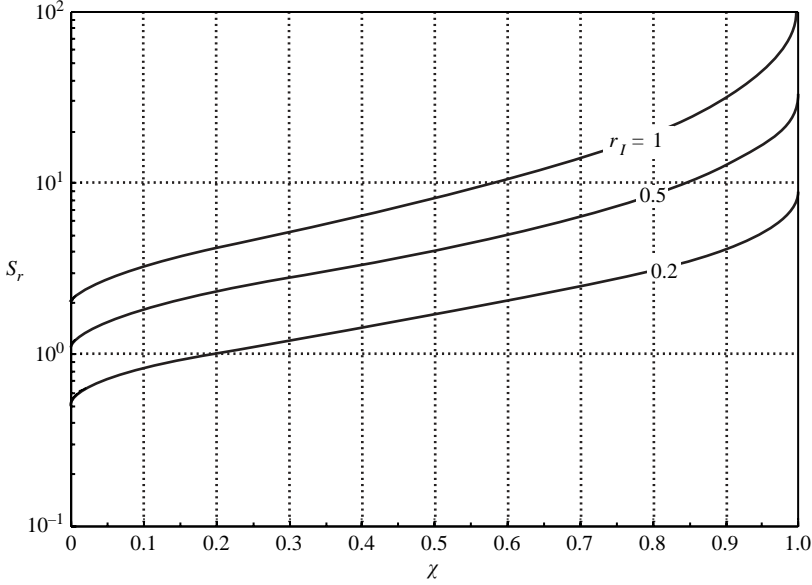


FIGURE 8. Variation of friction slope ratio along the channel with three different frictional ratios of r_l . The frictional parameter α is equal to unity.

non-dimensional form:

$$S_f = S_{fI} + S_{fb} = \frac{f_I G_0^2}{32y_1^3 y_2^3} + \frac{f_b G_0^2}{32y_2^3}. \quad (23)$$

The relative importance of interfacial and bottom friction can be determined by the ratio between their corresponding friction slopes, S_r ,

$$S_r \equiv \frac{S_{fI}}{S_{fb}} = \frac{(f_I G_0^2)/(32y_1^3 y_2^3)}{(f_b G_0^2)/(32y_2^3)} = r_l \left(1 + \frac{y_2}{y_1}\right)^3 = 8r_l \left(\frac{1}{1-2\eta}\right)^3 \quad (24)$$

The friction slope ratio, S_r , varies along the length of the channel. At the left-hand end of the channel ($\chi = 0$), for example, the friction slope ratio is least because the lower layer is thinnest there. The reduced lower layer thickness means intensified lower layer flow, and increased bottom friction. While at the right-hand end of the channel ($\chi = 1$), the friction slope ratio is greatest. The variation of the frictional slope ratio throughout the channel for three different frictional ratios is shown in figure 8. Even with $r_l = 0.2$, $S_r > 1$ along most of the channel, i.e. interfacial friction dominates bottom friction even when the bottom friction factor is five times larger than the interfacial friction factor.

6.2. Variation in interface height

As a first approximation Anati *et al.* (1977) and others have assumed a linear variation in interface height linking the hydraulic controls at each end of the channel. However, the analytical solution and laboratory experiments show that, while the variation is almost linear in the middle of the channel, it is curved at both ends as the flow approaches its hydraulic controls. The analytical solution shows that the density interface is not only nonlinear, but also asymmetric. This is because for open-channel exchange flows there is bottom friction acting upon the lower layer, but surface friction is assumed to be absent. For comparison purposes, the variations in interface

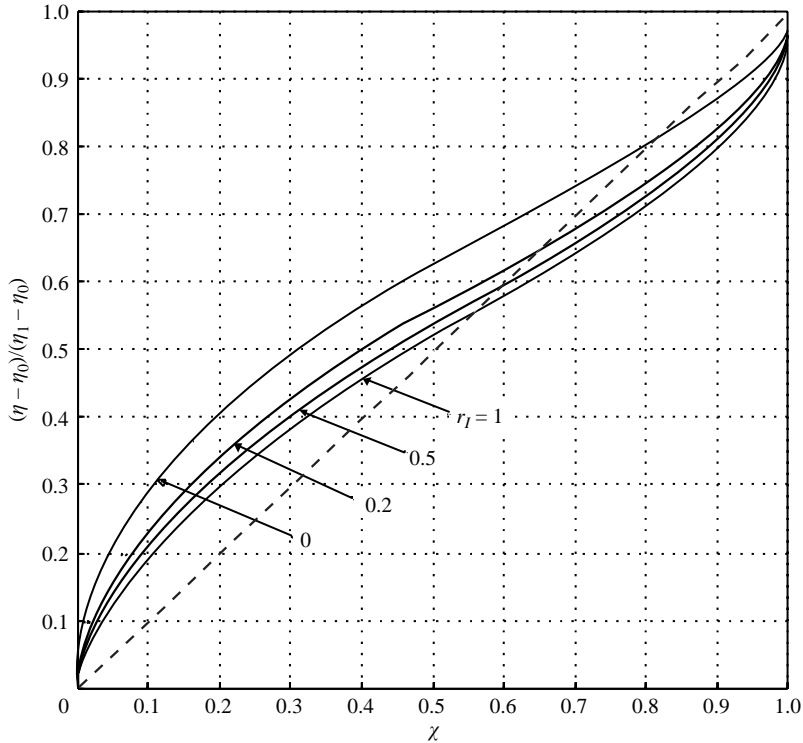


FIGURE 9. Normalized interface shapes throughout the channel for maximal exchange flows with varying frictional ratio r_I . The dotted line represents a linear interface profile and the frictional parameter α is equal to unity.

height have been normalized with respect to the interface heights at each end of the channel. The results for $r_I = 0.0, 0.2, 0.5$ and 1.0 are plotted in figure 9.

Given the absence of surface friction, the interface is always above mid-depth at the centre of the channel. The interface is more curved near the left-hand end of the channel than at the right, because the bottom friction increases as the thinner lower layer exits the channel. Both these effects become more pronounced as the relative importance of bottom friction increases, i.e. as r_I decreases. The interface is at mid-depth when $\chi = 0.46, 0.44$ and 0.41 for $r_I = 1.0, 0.5$ and 0.2 , respectively.

7. Conclusions

An analytical solution has been found for two-layer frictional exchange flow through a wide rectangular channel. This solution is based on the direct integration of the fully nonlinear one-dimensional shallow-water equation including both inertial and frictional effects. As a result, the solution is applicable to a wider range of flow conditions than both inviscid and linear frictional exchange flow solutions. Within the uncertainty of interfacial friction, the theoretical predictions of the analytical solution compare well with both laboratory experiments and field flow measurements in the Burlington Ship Canal.

Both interfacial and bottom friction are important in determining the exchange flow rate. The resulting exchange flow solutions indicate dramatic exchange flow rate reductions with increasing frictional effects. Consequently, frictional effects should not

be ignored even for very small values of the frictional parameter $\alpha = f_b L/H$. The analytical exchange flow solution indicates that the interface profile is not only nonlinear, but also asymmetric in nature. This asymmetry is due to the presence of bottom, but not surface, friction in open-channel exchange flows. The degree of asymmetry is strongly influenced by the relative importance of interfacial friction.

Funding from the Natural Sciences and Engineering Research Council of Canada (NSERC) is gratefully acknowledged. G. A. L. is grateful for support provided by the Canada Research Chairs program.

Appendix. Removal of the restriction $r_I = 1$

For simplicity, (12), (13) and (14) were presented for $r_I = 1$. The general expression for the variation in interface elevation (i.e. the extension of (12)) is:

$$\begin{aligned} \alpha G_0^2 \chi &= a_0 + a_1 \eta + a_2 \eta^2 + a_3 \eta^3 + a_4 \eta^4 + a_5 \ln \left(-\eta + r_I^{1/3} + \frac{1}{2} \right) \\ &+ a_6 \ln \left[\eta^2 + (r_I^{1/3} - 1) \eta + r_I^{2/3} - \frac{1}{2} r_I^{1/3} + \frac{1}{4} \right] + a_7 \tan^{-1} \left[\frac{-2\eta - r_I^{1/3} + 1}{r_I^{1/3} \sqrt{3}} \right], \end{aligned} \quad (\text{A } 1)$$

where a_0 is the constant of integration,

$$\begin{aligned} a_1 &= 4(8r_I + 1), \quad a_2 = 12, \quad a_3 = 16, \quad a_4 = 8, \\ a_5 &= 2 \left[G_0^2 (1 + r_I^{-1/3} + \frac{1}{3} r_I^{-2/3}) + \frac{16}{3} r_I^{1/3} (r_I^{1/3} + 1)^3 \right], \\ a_6 &= \left[G_0^2 (2 - r_I^{-1/3} - \frac{1}{3} r_I^{-2/3}) - 16 r_I^{1/3} (\frac{1}{3} r_I - 2r_I^{2/3} + r_I^{1/3} + \frac{1}{3}) \right], \\ a_7 &= \frac{2}{\sqrt{3}} \left[G_0^2 (-3r_I^{-1/3} + r_I^{-2/3}) + 16 r_I^{1/3} (r_I - 3r_I^{1/3} + 1) \right]. \end{aligned}$$

The general expression for the composite Froude number at the left-hand end of the channel (i.e. the extension of (13)) is:

$$G_0^2 = \frac{-8(8r_I + 1)\eta_0 - 32\eta_0^3 + \frac{32}{3} r_I^{1/3} (r_I^{1/3} + 1)^3 \phi_{01} - 16r_I^{1/3} (\frac{1}{3} r_I - 2r_I^{2/3} + r_I^{1/3} + \frac{1}{3}) \phi_{02} + \frac{32}{\sqrt{3}} r_I^{1/3} (r_I - 3r_I^{1/3} + 1) \phi_{03}}{\alpha - 2 \left(1 + r_I^{-1/3} + \frac{1}{3} r_I^{-2/3} \right) \phi_{01} - \left(2 - r_I^{-1/3} - \frac{1}{3} r_I^{-2/3} \right) \phi_{02} + \frac{2}{\sqrt{3}} (3r_I^{-1/3} - r_I^{-2/3}) \phi_{03}}, \quad (\text{A } 2)$$

$$\begin{aligned} \text{where } \phi_{01} &= \ln \left[\frac{\eta_0 + r_I^{1/3} + \frac{1}{2}}{-\eta_0 + r_I^{1/3} + \frac{1}{2}} \right], \\ \phi_{02} &= \ln \left[\frac{\eta_0^2 - (r_I^{1/3} - 1)\eta_0 + r_I^{2/3} - \frac{1}{2} r_I^{1/3} + \frac{1}{4}}{\eta_0^2 + (r_I^{1/3} - 1)\eta_0 + r_I^{2/3} - \frac{1}{2} r_I^{1/3} + \frac{1}{4}} \right], \\ \phi_{03} &= \tan^{-1} \left[\frac{4\sqrt{3} r_I^{1/3} \eta_0}{-4\eta_0^2 + 4r_I^{2/3} - 2r_I^{1/3} + 1} \right]. \end{aligned}$$

The general expression for the composite Froude number at the right-hand end of the channel (i.e. the extension of (14)) is:

$$G_0^2 = \frac{8(8r_I + 1)\eta_1 + 32\eta_1^3 + \frac{32}{3} r_I^{1/3} (r_I^{1/3} + 1)^3 \phi_{11} - 16r_I^{1/3} (\frac{1}{3} r_I - 2r_I^{2/3} + r_I^{1/3} + \frac{1}{3}) \phi_{12} + \frac{32}{\sqrt{3}} r_I^{1/3} (r_I - 3r_I^{1/3} + 1) \phi_{13}}{\alpha - 2 \left(1 + r_I^{-1/3} + \frac{1}{3} r_I^{-2/3} \right) \phi_{11} - \left(2 - r_I^{-1/3} - \frac{1}{3} r_I^{-2/3} \right) \phi_{12} - \frac{2}{\sqrt{3}} (3r_I^{-1/3} - r_I^{-2/3}) \phi_{13}}, \quad (\text{A } 3)$$

$$\text{where } \phi_{11} = \ln \left[\frac{-\eta_1 + r_I^{1/3} + \frac{1}{2}}{\eta_1 + r_I^{1/3} + \frac{1}{2}} \right],$$

$$\phi_{12} = \ln \left[\frac{\eta_1^2 + (r_I^{1/3} - 1)\eta_1 + r_I^{2/3} - \frac{1}{2}r_I^{1/3} + \frac{1}{4}}{\eta_1^2 - (r_I^{1/3} - 1)\eta_1 + r_I^{2/3} - \frac{1}{2}r_I^{1/3} + \frac{1}{4}} \right],$$

$$\phi_{13} = \tan^{-1} \left[\frac{-4\sqrt{3}r_I^{1/3}\eta_1}{-4\eta_1^2 + 4r_I^{2/3} - 2r_I^{1/3} + 1} \right].$$

REFERENCES

- ANATI, D. A., ASSAF, G. & THOMPSON, R. 1977 Laboratory models of sea straits. *J. Fluid Mech.* **81**, 341–351.
- ARITA, M. & JIRKA, G. H. 1987 Two-layer model of saline wedge. I: Entrainment and interfacial friction. *J. Hydraul. Engng ASCE* **113**, 1229–1247.
- ARMI, L. 1986 The hydraulics of two flowing layers of different densities. *J. Fluid Mech.* **163**, 27–58.
- ARMI, L. & FARMER, D. M. 1985 The internal hydraulics of the Strait of Gibraltar and associated sill and narrows. *Oceanol. Acta* **8**, 37–46.
- ARMI, L. & FARMER, D. M. 1986 Maximal two-layer exchange through a contraction with barotropic net flow. *J. Fluid Mech.* **164**, 27–51.
- ARMI, L. & FARMER, D. M. 1987 A generalization of the concept of maximal exchange in a strait. *J. Geophys. Res.* **92**, 14 679–14 680.
- ASSAF, G. & HECHT, A. 1974 Sea strait: a dynamic model. *Deep-Sea Res.* **21**, 947–958.
- BROWAND, F. K. & WINANT, C. D. 1973 Laboratory observations of shear-layer instability in stratified fluid. *Boundary-Layer Met.* **5**, 67–77.
- DEFANT, A. 1961 *Physical Oceanography*, vol. 1. Pergamon.
- DICK, T. M. & MARSALEK, J. 1973 Exchange flow between Lake Ontario and Hamilton Harbour. *Environment Canada, Canada Center for Inland Waters, Burlington, Ontario, Scientific Series*, no. 36.
- FARMER, D. M. & ARMI, L. 1986 Maximal two-layer exchange over a sill and through the combination of a sill and contraction with barotropic flow. *J. Fluid Mech.* **164**, 53–76.
- GARRETT, C. & GERDES, F. 2003 Hydraulic control of homogeneous shear flows. *J. Fluid Mech.* **475**, 163–172.
- GREGG, M., ÖZSOY, E. & LATIF, M. 1999 Quasi-steady exchange flow in the Bosphorus. *Geophys. Res. Lett.* **26**, 83–86.
- GU, L. 2001 Frictional exchange flow through a wide channel with application to the Burlington Ship Canal. PhD thesis, University of British Columbia.
- HENDERSON, F. M. 1966 *Open Channel Flow*. Macmillan.
- LAWRENCE, G. A. 1993 The hydraulics of steady two-layer flow over a fixed obstacle. *J. Fluid Mech.* **254**, 605–633.
- LAWRENCE, G. A., BROWAND, F. K. & REDEKOPP, L. G. 1991 The stability of a sheared density interface. *Phys. Fluids A Fluid Dyn.* **3**, 2360–2370.
- LAWRENCE, G. A., HAIGH, S. P. & ZHU, Z. 1998 In search of Holmboe's instability. *Physical Processes in Lakes and Oceans* (ed. J. Imberger), pp. 295–304. American Geophysical Union, Washington.
- LAWRENCE, G. A., PIETERS, R., ZAREMBA, L. J., TEDFORD, E., GU, L., GRECO, S. L. & HAMBLIN, P. F. 2004 Summer exchange between Hamilton Harbour and Lake Ontario. *Deep-Sea Res.* **51**, 475–487.
- OĞUZ, T., ÖZSOY, E., LATIF, M. A., SUR, H. I. & ÜNLÜATA, Ü. 1990 Modeling of hydraulically controlled exchange flow in the Bosphorus strait. *J. Phys. Oceanogr.* **20**, 945–965.
- OTTESEN-HANSEN, N. & MOELLER, J. 1990 Zero blocking solution for the Great Belt Link. In *The Physical Oceanography of Sea Straits* (ed. L. Pratt), pp. 153–170. Kluwer.
- SARGENT, F. E. & JIRKA, G. H. 1987 Experiments on saline wedge. *J. Hydraul. Engng ASCE* **113**, 1307–1324.

- SCHIJF, J. & SCHÖNFELD, J. 1953 Theoretical considerations on the motion of salt and fresh water. *Proc. of the Minn. Intl Hydraulics Conv.* pp. 321–333.
- SMEED, D. A. 2004 Exchange through the Bab el Mandab. *Deep-Sea Res.* **51**, 455–474.
- STEVENS, C. & COATES, M. J. 1994 Applications of a maximized cross-correlation technique for resolving velocity fields in laboratory experiments. *J. Hydraul. Res.* **32**, 195–212.
- TURNER, J. S. 1973 *Buoyancy Effects in Fluids*. Cambridge University Press.
- WOOD, I. R. 1970 A lock exchange flow. *J. Fluid Mech.* **42**, 671–687.
- ZAREMBA, L. J., LAWRENCE, G. A. & PIETERS, R. 2003 Frictional two-layer exchange flow. *J. Fluid Mech.* **474**, 339–354.
- ZHU, D. Z. & LAWRENCE, G. A. 2000 Hydraulics of exchange flows. *J. Hydraul. Engng ASCE* **126**, 921–928.
- ZHU, D. Z. & LAWRENCE, G. A. 2001 Holmboe's instability in exchange flows. *J. Fluid Mech.* **429**, 391–409.